Buckling capacity model for timber screws loaded in compression: Experimental, analytical and FE investigations

Buckling capacity model for compressed timber screws: experimental, analytical and FE investigations

Angelo Aloisio[a,b,*], Matteo Pelliciari[c], Yuri De Santis[a], Marco Martino Rosso[d], Massimo Fragiacomo[a], Roberto Tomasi[b]

[a] *Department of Civil Engineering, University of L'Aquila, Italy*
[b] *Faculty of Science and Technology, Norwegian University of Life Sciences, Norway*
[c] *Department of Engineering "Enzo Ferrari", Università degli Studi di Modena e Reggio Emilia, 41125 Modena, Italy*
[d] *Politecnico di Torino, DISEG, Department of Structural, Geotechnical and Building Engineering, Corso Duca Degli Abruzzi, 24,Turin 10128 Italy*

Abstract

This paper investigates the buckling of compressed screws inserted into timber members. Screws are often used as a reinforcement in timber structures. Under compression forces, they are prone to axial buckling. The current model for the screw buckling, enclosed in the EC5 proposal, is based on the general framework of EC3 for the instability of compressed steel members. The main shortcomings of the current formulation for the buckling of screws are the following. (1) The analytical expression for calculating the theoretical buckling load does not follow the observed buckling modes. (2) Due to the lack of dedicated studies, the value of the imperfection coefficient is arbitrarily chosen. This paper fills the above gaps. Firstly, a simple analytical expression for predicting the buckling of screws is proposed and validated against experimental and finite element (FE) findings. The formulation adopts a more accurate expression for the lateral deformation, based on experimental observation. Secondly, a FE model calibrated on experimental buckling tests is used to estimate the defect coefficients of the instability curves as a function of the amplitude of the geometric defects of the screw, expressed as a fraction of its length. A Markov chain Monte Carlo analysis is carried out to simulate the capacity of screws with different lengths and diameters, assuming the uncertainty of all input parameters sampled from suitable probability distributions. The results are used to validate the proposed deterministic capacity model and estimate the uncertainty factors of the design equation.
Keywords: Screws; Buckling; Timber; Compression perpendicular to grain; Experimental tests; Analytical model; FE validation

May 25, 2023

List of symbols and notations

- A: Area of the section of the screw.
- A_{imp}: Amplitude of the geometric imperfection of the screw defined in Fig. 7.
- α: Angle between screw axis and grain direction of the wood.
- α_g: Imperfection coefficient in Eq. (3) defined for steel members in Tab. 3.
- β: Constant appearing in Eq. (A.8) defined as $(c_v/EA)^{0.5}$.
- $c_h = (0.19 + 0.012d)\,\rho\left(\frac{90°+\alpha}{180}\right)$: Horizontal sub-grade coefficient for the screw for solid timber, glued laminated (GL) timber of softwood. c_h is in MPa if d is in mm, ρ in kg/m^3 and α in degrees.
- $c_{v,exp} = 234\frac{(\rho d)^{0.2}}{l_w^{0.6}}$: Horizontal sub-grade coefficient for the screw for solid timber, glued laminated (GL) timber of softwood. c_v is in MPa if d is in mm, ρ_k in kg/m^3.
- c_v: Horizontal sub-grade coefficient for the screw used in Eq. (A.8).
- CoV: Coefficient of variation.
- CPG: Compression perpendicular to the grain.
- d: Outer thread diameter of the screw.
- d_1: Inner thread diameter of the screw estimated as $0.5d$.
- ϵ: Standard normal distribution.
- E: Young's modulus of steel equal to 210 GPa (*).
- F_w: Withdrawal capacity of the screw (*).
- f_w: Withdrawal strength of the screw (*).
- F_c: Axial capacity of the screw (*).

*Corresponding author.
Email addresses: angelo.aloisio1@univaq.it (Angelo Aloisio), matteo.pelliciari@unimore.it (Matteo Pelliciari), yuri.desantis@univaq.it (Yuri De Santis), marco.rosso@polito.it (Marco Martino Rosso), massimo.fragiacomo@univaq.it (Massimo Fragiacomo), roberto.tomasi@nmbu.no (Roberto Tomasi)

May 25, 2023

- $F_{fem,\mathrm{NLSIM}}$: Axial capacity of the screw from the FE model assuming an initial geometric imperfection (*).
- F_{exp}: Experimental capacity of the screw estimated as the maximum of the experimental curve.
- f_y: Yielding strength of the steel (*).
- $k = 0.5\left[1 + 0.49\left(\bar{\lambda} - 0.2\right) + \bar{\lambda}^2\right]$: Buckling coefficient for the screws.
- k_c: Proposed reduction coefficient of the yielding strength of the screw.
- $\kappa_c = \begin{cases} 1, & \bar{\lambda} \leq 0.2 \\ \frac{1}{k+\sqrt{k^2-\bar{\lambda}^2}}, & \bar{\lambda} > 0.2 \end{cases}$: Reduction factors for screw buckling. Alternatively, the values in Tab. 1 can be used. For values not included in Tab. 1 a linear interpolation should be carried out.

Table 1: Reduction factors due to buckling, where α is the angle between screw axis and grain.

f_{yk} [Mpa]	α=90	α=0
1000	0.6	0.5
800	0.65	0.55
500	0.75	0.65

- I: Moment of inertia of the screw estimated as $(\pi d_1^4/64)$.
- K_{ax}: Axial stiffness of the screw.
- l: Total length of the screw.
- l_r: Penetration part of the threaded part of the screw.
- $\bar{\lambda} = \frac{N_{pl}}{N_{ki}}$: Relative slenderness ratio of the screws (*).
- m: Order of the sine function associated with the first buckling mode in Eq. (A.6)
- n: Number of fully threaded screws.
- n_0: Number of fully threaded screws or rods arranged in a row parallel to the grain.
- N_{pl}: Characteristic yielding strength of the screw (*).
- $N_{ki} = 2\sqrt{c_h EI}$: Approximate ideal elastic buckling of a Winkler beam (*).

- N_w: Ideal elastic buckling of a Winkler beam, expressed by Eq. (A.5) (*).
- N_p: Proposed theoretical elastic buckling of a Winkler beam, given by Eq. (17) (*).
- $N_{fem,buck}$: Ideal elastic buckling of a screw estimated with the FE model (*).
- ξ: Reciprocal of the fraction of the screw length which represents the geometric imperfection defined in Eq. (18).
- ρ: Density of wood (*).
- σ_h: Standard deviation of the empirical regression for c_h in Eq. (7) estimated from [1] and defined in Tab. 8.
- σ_v: Standard deviation of the empirical regression for c_v in Eq. (A.12) estimated from [1] and defined in Tab. 8.
- $u(x)$: Axial displacement of the screw as a function of the abscissa x.
- $v(x)$: Transverse displacement of the screw as a function of the abscissa x.
- γ_R: Partial factor for material property.
- γ_{M1}: Partial factor for a design resistance based on a (semi) empirical analysis with a ductile failure mode.

(*) The addition of a subscript k indicates the corresponding characteristic value.

1. Introduction

The increasing importance of mass timber structures is also related to the development of self-tapping screws (STS) [2]. STS is growing as the leading fastener system in timber engineering, used in timber-to-timber [3–5], steel-to-timber [6, 7] and concrete-to-timber [8, 9]. An STS consists of three main components: the head (sunk or non-sunk), thread (full or partial) and self-drilling tip [10–12]. STS are often used as reinforcements to prevent failure mechanisms associated with compression perpendicular to the grain (CPG), shear stresses [9, 13, 14], or tensile stresses perpendicular to grain [4, 10, 15], see the screw reinforcement around holes in timber beam [16–18, 18–21].

Mainly to avoid excessive local deformation, the screws are used to reinforce timber members under CPG [11, 22]. In this case, the screws are subjected to axial forces applied at the screw head. There are standard design approaches for timber under CPG, mainly originating from [23, 24]. The standard capacity model for timber reinforced with screws is additive [25, 26]. The capacity is the summation between the wood and screw resistance. The timber CPG strength has been extensively investigated since 1929 by Swenson; see also the studies by Kollmann and Coté [27], Graf [28] and Suenson [29], Gehri [30] and Hübner [31], Gaber [32], Frey-Wesseling and Stüssi [33], Rothmund [34], Hoffmeyer et al. [35]. There are well-consolidated models, empirical, mechanics-based, and probabilistic [36, 37]. Conversely, less research was directed to the screw capacity characterization under axial force.

The screw capacity is estimated as the minimum between the push-in and buckling resistance. The push-in resistance is straightforward to evaluate since it can be estimated by multiplying the withdrawal strength by the screw surface. Besides, due to the symmetry between push-in and withdrawal behaviour, there are extensive experimental campaigns for its resistance and stiffness characterization: studies on withdrawals can be considered valid also for push-in. Conversely, the buckling model has never been investigated systematically.

The buckling model for the screws originates from the DIN [15] and corresponds to the general framework in the EC3 [38] for compressed steel members. It evaluates the buckling load as the product between the plastic resistance and the buckling reduction factor, a function of the theoretical buckling load. Given the general framework for compression buckling, Bejtka [1] observed that the buckling load is difficult to obtain with a closed-forced analytical expression and complied tables for the buckling load based on FE analyses in Ansys. The current EC5 proposal acknowledges the difficulty of using tables or FE to calculate the theoretical buckling load. Therefore, it estimates the buckling using a simplified expression valid for beams embedded in an elastic subgrade under a constant axial force. Despite the severe limitations, approximations and inaccuracy of the model, the predictions agree with the experimental results. However, as later discussed, this agreement depends on the low sensitivity of the buckling model to the theoretical buckling load rather than on the reasonable acceptability of the inherent model assumptions.

No paper attempts to critically discuss the buckling model for screws based on FE or

analytical investigations. Additionally, despite the considerable research in pile modelling, there has never been exchanging of knowledge between geotechnics and timber engineering. The review by Poulos and Davis [39] shows that the buckling studies on slender piles range from the 1929 analysis by Granholm [40], who utilized the Winkler foundation for representing the soil response, to more recent computer analysis, which uses the elastic continuum as a soil model. However, the main limitations of existing analytical models are that foundation is homogeneous, and the loading is concentrated at the extremities of the pile [41–43].

The analytical solutions proposed by Hetenyi [41] and Timoshenko and Gere [44] should not be considered valid for screws, since the axial force is not constant and vanishes at the screw tip. Likewise, Terzaghi affirmed that, also in geotechnics, there are circumstances where the analytical solutions cannot be considered valid [45]. For piles, the primary source of inaccuracy is the uncertainty of the subgrade reaction characterization [46, 47]. The error associated with a mistaken soil characterization can be considered more critical than the modelling error. Therefore, it is generally accepted that the Winkler model does provide a reasonably accurate method for estimating the lateral response of piles [48]. Despite the general acceptance of the classical Winkler model [49], there is advanced research on pile stability accounting for a nonuniform axial force. For instance, Heelis [50] studied the stability of piles supported vertically by a frictional force. Nonetheless, the intrinsic uncertainty of the soil characteristics makes it difficult to transfer knowledge from structural mechanics to geotechnical design [51].

Conversely, the subgrade reaction in the screws is known with higher accuracy than the soil [1]. Considerable research aimed to characterize the horizontal and vertical subgrade reactions in screws was carried out. The estimation of the vertical subgrade reaction is associated with studies on the withdrawal properties of STS. Initial investigations by Blaß et al. [52] led to an empirical equation for predicting withdrawal stiffness as a function of the wood density, screw diameter and penetration length. The empirical model was later modified by Ringhofer et al. [53] based on more extensive testing, considering the influence of laminated timber products (e.g., GLT, CLT) and thread of the screws (e.g., fully and partially threaded). Recently, Stamatopoulos and Malo [54] developed a withdrawal stiffness equation that accounts for the influence of grain angle. Even with the above mod-

ifications [54], the model for the axial stiffness leads to less accurate results than models for the lateral stiffness. For instance, the model by Bejtka yielded an R^2 close to 0.6 for the axial stiffness.

Conversely, the horizontal subgrade reaction, known as embedment stiffness, can be predicted with higher accuracy [55, 56]. Bejtka obtained an R^2 higher than 0.9 using simple empirical regression. The current Eurocode 5 [57] only provides the lateral stiffness for bolted connections expressed as a function of wood density and dowel diameter. However, the EC5 proposal encloses an expression for the lateral stiffness of the screws following Bejtka [52]. Bejtka proposed an expression for predicting the embedment stiffness as a function of the wood density, screw diameter and insertion angle. The embedment and axial stiffness are both needed for rigorous mechanics-based screw models [58]. Nonetheless, the above empirical regressions were mainly used to evaluate stiffness properties [59] rather than refining or analyzing the buckling model of screws.

Given the satisfactory accuracy of the empirical regressions for the lateral and axial subgrade reaction, improving the current buckling model for screws is reasonable. Moreover, different from geotechnics, the lower uncertainty of the embedment stiffness makes it reasonable to reduce the modelling error. So far, the main obstacle against the development of the model was the lack of a free database of experimental tests on buckling screws, despite the numerous tests carried out in the past [60]. To the authors' knowledge, no paper attempts to reduce the modelling error for predicting the buckling of the screws using a rigorous mechanics-based formulation.

The objectives and novelties of this paper are the following:

- Theoretical derivation of an analytical equation for estimating the buckling load of screws based on the observed buckling mode.
- Experimental tests on compressed screws to observe the buckling failure mode and assess the related capacity.
- FE modelling of the tested configurations used to (i) validate the theoretical buckling load estimated using the proposed equation and (ii) calibrate the effect of the initial geometric defect on the capacity.

- Markov chain Monte Carlo analyses [61] to assess the screw buckling capacity as a function of all input parameters, with their inherent uncertainty sampled from suitable probability distributions, given different values of the initial geometric imperfection.

- Calibration of the defect coefficients of the improved deterministic model for the buckling capacity of the screws as a function of the initial screw imperfection. The defect coefficients' estimations guarantee the general applicability of the model valid for any assumption of the initial defect. Additionally, the authors estimate the uncertainty factors of the corresponding design equations.

The paper comprises four main parts: experimental tests (Section 3), analytical derivation (Section 4), FE model calibration (Section 5), and Monte Carlo simulations (Section 6). Section 2 explains the paper's methodology, introducing the reader to the following investigations. The section on experimental tests is reported before the analytical and FE models to give the reader a physical understanding of the buckling failure modes observed in actual screws. The observation of the buckling modes will be used to develop the analytical formulation for the instability problem.

2. Problem formulation and methodology

In 2012, the European Committee for Standardization (CEN) made a program to develop the second generation of Eurocodes, including new materials, products, and construction methods [62]. Eurocode 5 - design of timber structures, NS-EN 1995-1-1, includes a buckling model for screws. The working draft, prEN 1995 of November 2021, reports a set of equations for calculating the axial resistance of the screws, summarized in the synoptic Tab. 2. A detailed definition of the notation is given at the beginning of the paper.

The buckling model for timber screws under compression in Tab. 2 originates from the standard DIN 18800 [1] and coincides with the general formulation valid for axial buckling of steel members reported in the current EC3 [38, 63]. Estimating the axial resistance requires the computation of two inputs, the theoretical buckling load and the plastic resistance, as shown in Fig. 1. The theoretical buckling load expresses the ideal buckling force without defects. At the same time, plastic resistance is the axial resistance

Table 2: Synoptic table on the standard model for the buckling capacity of timber screws.

Buckling resistance of the screws (prEN 1995-1-1)

$$F_c = k_c N_{pl} \tag{1}$$

$$\kappa_c = \begin{cases} 1, & \bar{\lambda} \leq 0.2 \\ \frac{1}{k+\sqrt{k^2-\bar{\lambda}^2}}, & \bar{\lambda} > 0.2 \end{cases} \tag{2}$$

$$k = 0.5\left[1 + \alpha_g\left(\bar{\lambda} - 0.2\right) + \bar{\lambda}^2\right] \text{ where } \alpha_g = 0.49; \text{ See Tab.3} \tag{3}$$

$$\bar{\lambda} = \left(\frac{N_{pl}}{N_{ki}}\right)^{0.5} \tag{4}$$

$$N_{pl} = \pi \frac{d_1^2}{4} f_y \tag{5}$$

$$N_{ki} = 2\sqrt{c_h EI} \ (^*) \tag{6}$$

$$c_h = (0.19 + 0.012d)\,\rho\left(\frac{90^\circ + \alpha}{180}\right) \tag{7}$$

(*) See Appendix C for further details on the choice of N_{ki}.

of the element in the absence of instability phenomena. The ideal buckling never occurs due to initial imperfections, which reduce the theoretical buckling load. Therefore, the classical formulation assumes the resistance as the product between the plastic resistance and a buckling reduction coefficient, see Eq. (1). The buckling coefficient in Eq. (2) is different than one only for screws with relative slenderness higher than 0.2, where the slenderness in Eq. (4) is computed as the ratio between the plastic (Eq. (5)) and the ideal buckling force (Eq. (6)).

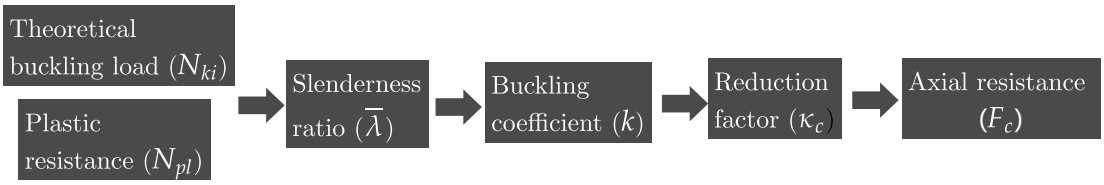

Figure 1: Illustration of the steps needed for the computation of the compression resistance of timber screws.

The model in Tab. 2 is not specific to the screws but comes from the traditional mathematical framework for instability phenomena. The model in Tab. 2 has been applied as it is to the screws with two modifications:

- Adopting Eq. (6) for estimating the ideal buckling load of the screws.
- Assuming a constant defect class c for the screws, with the corresponding defect

coefficient equal to 0.49 [38].

The first assumption is incorrect since the solution in Eq. (6) has several limitations; the most relevant is the buckling mode. The buckling mode corresponding to Eq. (6) is a simple sine. However, experiments show that the buckling of the screw takes place with a concentration of the deformation in the region close to the point where the external load is applied. The deformation tends to vanish rapidly; thus, a simple sine is not appropriate to describe such buckled mode. All the assumptions of Eq. (6) are discussed in-depth in Appendix A. The following limitations of the buckling formulation are highlighted:

1. The deformed shape is a simple sine, which does not reflect the buckling mode of a screw inserted in an elastic medium. A damped sine is more appropriate.

2. Eq. 6 does not respect the boundary conditions for a pinned-pinned beam assumed in the formulation [44, 64].

3. The axial force is assumed constant along the axis of the screw, and the axial stiffness is infinite.

Regarding the second aspect, there are no studies relating the screw defects to the imperfection coefficients. Additionally, the substantial difference between the buckling mode of compressed steel members (a sine) and the screw (a damped sine) compromises the direct application of the imperfection coefficients of EC3 to the screws.

Therefore, the model in the synoptic Tab. 2 might need the twofold enhancements:

- An expression for the theoretical buckling load based on a suitable assumption for the buckling mode.

- Calibration of the geometric uncertainty factors (α_g), appearing in Eq. (3) as a function of the initial geometric imperfection. The EC5 proposal assumes $\alpha_g = 0.49$, corresponding to a class c in Tab. 3. However, this parameter has never been calibrated on the screws for different values of the initial geometric defect. The values in Tab. 3 cannot be directly used for the screws since the buckling mode of the screws is significantly different from a sine.

Table 3: Values of the geometric imperfection factor (α_g) for various stability curves.

Stability curve	a_0	a	b	c	d
α_g	0.13	0.21	0.34	0.49	0.76

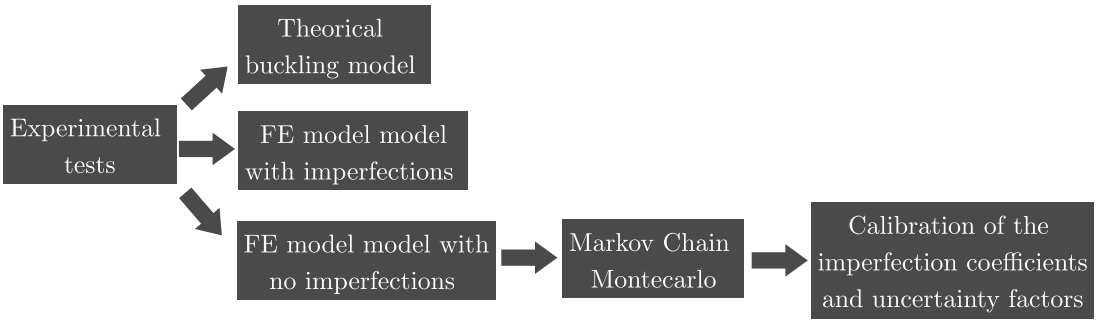

Figure 2: Workflow of the investigation carried out in this paper.

As illustrated in Fig. 2, the investigation consists of two main steps, almost independent of each other. The problem is tackled by analysing and discussing experimental tests on compressed screws. The analyses reveal the buckling modes and provide the actual capacity of the screws. The first step in Section 4 is deriving a theoretical formulation for the critical buckling load. The formulation is based on an assumption of the buckled shape from experimental evidence. The model is validated against the theoretical buckling loads obtained from the FE model. The second step deals with the FE investigation considering the effect of geometric defects. This step consists of three phases:

- Development of a linear FE model of the compressed screws, representing the experimental configurations, for estimating the theoretical buckling loads and the related buckling modes. In this phase, the authors validate the analytical expression for the theoretical buckling and compare the experimental, FE and analytical predictions for the buckling modes.

- Calibration of the geometric defect of the screws using the experimental data. The axial capacity is obtained from a quasi-static nonlinear push-in analysis of the screws, assuming an initially deformed configuration corresponding to the first buckling mode, estimated from the solution of the linear instability problem. In this phase, the authors compare the FE predictions for the axial capacity and the corresponding experimental values.

- Markov chain Monte Carlo (MCMC) analyses [61] of the push-in FE simulations assuming the uncertainties of all input parameters obtained by sampling suitable probability distributions, given different values for the initial geometric imperfection. This section aims to estimate the geometric uncertainty factor in Eq. (3) given different amplitudes for the initial geometric imperfection, expressed as a fraction of the screw length. Additionally, the MCMC analyses lead to an estimate of the uncertainty safety factors of the corresponding design equations. It must be remarked that for the first time, the values for α_g are estimated for timber screws.

3. Experimental tests

The authors conducted compression tests on a set of timber screws used for validating the FE model of the screw and understanding the physics behind the buckling of the screws. The screw has been directly loaded by connecting a Torx bit to the load cell through a steel plate. The steel plate and Torx bit used for the tests are shown in Fig. 4. The test specimens are glue-laminated timber of strength class GL30c (ρ_k=390 kg/m^3, ρ=430 kg/m^3), with dimensions of 800 x 140 x 225 or 1200 x 140 x 540 mm (length x width x height). Rothoblaas produced the screws. The mean moisture content of the specimens measured by a Delmhorts RDM3 instrument was 12.3%. Fig. 3 and Tab. 4 show a schematic overview of the different screws, where l_r is the effective screw length applied in the design model. The column named "Head" describes the geometry of the screw head. The predicted failure mode is according to the design model. The screws are fully

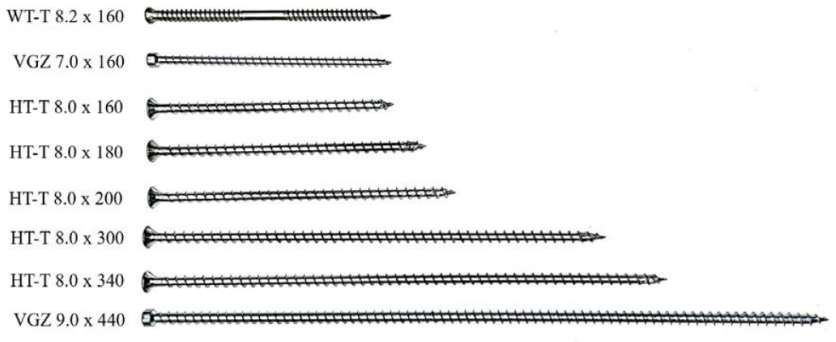

Figure 3: View of the tested screws.

threaded self-tapping screws, except for the WT-T screw, which is double-threaded. They

Table 4: Screw type

Screw type	Head	Diameter [mm]	Length [mm]	l_r [mm]	Predicted failure	Height [mm]
VGZ	Cylindrical	7	160	160	Buckling	225
WT-T	Cylindrical	8.2	160	130	Push-in	225
HT-T	Countersunk	8	160	160	Buckling	225
HT-T	Countersunk	8	180	180	Buckling	225
HT-T	Countersunk	8	200	200	Buckling	225
HT-T	Countersunk	8	300	300	Buckling	540
HT-T	Countersunk	8	340	340	Buckling	540
VGZ	Cylindrical	9	440	440	Buckling	540

were drilled with a right angle, and the head was flushed in the timber surface. The screw is compressed using a load cell of the ZwickRoell Z1200 UTM (Universal Testing Machine). The loading protocol detailed in [11] consists of three phases following EN408 and ISO6891.

(a) (b)

Figure 4: Setup of specimen with height 540 mm in ZwickRoell Z1200-Steel plate used for Torx tests- Setup of Torx test.

Phases 1 and 2 follow ISO6891 and aim to avoid initial residual deformations and stabilize the loading area. The specimen is loaded up to 40% of the estimated resistance (F_c), held for 30 seconds before the load decreases to 10% of F_c, and then held for 30 seconds. The load rate in phases 1 and 2 is determined as the ratio between 40% and 10% of F_c respectively, and 60 seconds. The actual load-displacement curves used in the analyses correspond to phase 3. Phase 3 follows EN408. Hence, the maximum force will be reached within 300 ± 120 seconds.

The authors carried out in total sixteen tests, eight configurations and each with two repetitions. Fig. 5 displays the force-displacement curves. The capacity is estimated as the curve's maximum; see Fig. 5(b). The trend is almost linear up to the attainment of the resistance. Then, there is a sudden, almost vertical drop due to the attainment of the

buckling load.

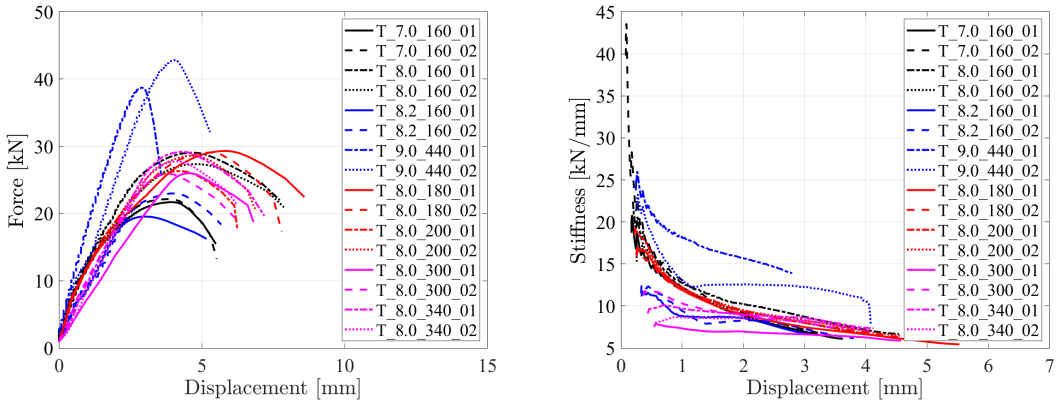

(a) (b)

Figure 5: Load-displacement (a) and Stiffness-displacement (b) curves.

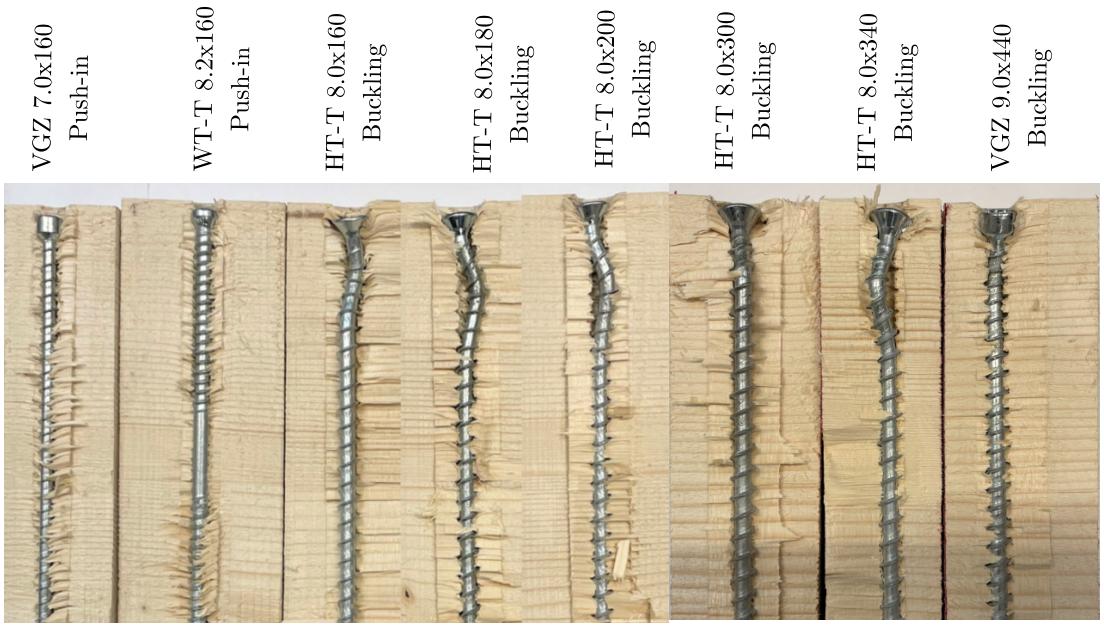

Figure 6: Failure modes of the tested screws.

Six out of the eight screws failed due to axial instability; see Fig. 6 showing typical buckling modes. Tab. 5 reports the experimental and predicted capacity using Eq. (1). The discrepancies between the predictions and the estimates are:

- The failure mode is always buckling, except for the short screws VGZ 7.0x160 and WT-T 8.2x160.
- The relative error between the predictions using Eq. (1) and the experimental values

is higher than 100%. Although this difference might appear irrelevant for a single screw in absolute values, it might be more significant when dealing with reinforcements using multiple screws.

Table 5: Comparison between experimental and predicted capacity, where $F_{exp,1}$ and $F_{exp,2}$ are the experimental capacities of the first and second test repetition, F_{exp} is the mean between $F_{max,1}$ and $F_{exp,2}$, F_c is the predicted value according to EC5 in kN based on Tab. 2.

Screw type	d [mm]	l_r [mm]	$F_{exp,1}$	$F_{exp,2}$	F_{exp}	F_c Eq. (1)	Error [%]	Exp. Fail.	Pred. Fail.
VGZ	7	160	21.7	22.1	21.9	9.7	126.6%	Push in	Buckling
WT-T	8.2	130	19.6	23.0	21.3	13.4	58.9%	Push in	Buckling
HT-T	8	160	29.1	27.4	28.2	12.7	121.6%	Buckling	Push in
HT-T	8	180	29.3	29.1	29.2	12.7	129.3%	Buckling	Buckling
HT-T	8	200	26.3	28.6	27.5	12.7	115.7%	Buckling	Buckling
HT-T	8	300	26.0	25.9	26.0	12.7	103.9%	Buckling	Buckling
HT-T	8	340	29.2	27.8	28.5	12.7	123.8%	Buckling	Buckling
VGZ	9	440	38.7	42.8	40.8	16.2	151.3%	Buckling	Buckling

The deformation of the buckling mode is localized at the screw head. The head almost remains aligned with the screw axis. Right after the head, the screw exhibits a single bend, while the remaining part of the screw is almost undeformed. The shape of the buckling mode mainly depends on the stress localization at the screw head, as discussed in the appendix (see Eq. (A.11)). The observed buckling mode is far different from that assumed in the estimation of Eq. (6), corresponding to a simple sine [44].

4. Proposed theoretical formulation for the critical buckling load

As previously mentioned, the classical solution to the buckling problem of a bar on an elastic foundation is derived by assuming a simple sine as buckled shape. However, the experiments show that the actual deformed shape exhibits a sinusoidal trend close to the loaded end of the screw. Right after, the deflection smoothly decreases. Thus, it seems more appropriate to assume a damped sine for the buckled shape. In the following, this assumption will be adopted to propose a more accurate theoretical solution for the buckling of screws.

The solution to the buckling problem of a bar on an elastic foundation is derived under the following hypotheses: (i) the bar has an infinite axial stiffness; (ii) the ends of the bar are hinged; (iii) the variation of axial load along the longitudinal axis is neglected. Comments

on this last hypothesis are given in Appendix A.2. Following the energy method, the critical value of the load can be found by minimizing the deformation energy [44], namely

$$\Delta U = \Delta T \tag{8}$$

where ΔU is the strain energy and ΔT is the external work.

The theoretical buckling load of a Winkler beam, expressed by Eq. (6), was derived by assuming the following buckled shape [44]:

$$v(x) = c \sin\left(\frac{m\pi x}{l_r}\right) \tag{9}$$

In light of the previous considerations, a simple sine is not suitable for the description of the actual buckled shape of the bar. Hence, we adopt instead a damped sine, expressed as

$$v(x) = c\, e^{-\frac{m}{l_r}x} \sin\left(\frac{m\pi x}{l_r}\right) \tag{10}$$

The strain energy of the buckled bar is the sum of the energy associated with the bending and the subgrade deformation:

$$\Delta U = \Delta U_1 + \Delta U_2 \tag{11}$$

where

$$\Delta U_1 = \frac{EI}{2} \int_0^{l_r} v''(x)^2 dx = \frac{EI\left(5+\pi^2\right)\pi^2 c^2 e^{-m} m^3 \sinh(m)}{4{l_r}^3} \tag{12}$$

The lateral reaction of an element dx of the bar is $c_h v dx$. Hence, the total strain energy of the elastic medium is

$$\Delta U_2 = \frac{c_h}{2} \int_0^{l_r} v^2(x) dx = \frac{c_h \pi^2 c^2 l_r\, e^{-m} \sinh(m)}{2\left(2\pi^2 m + 2m\right)} \tag{13}$$

The work done by the axial force in the critical configuration is

$$\Delta T = \frac{N_{cr}}{2} \int_0^{l_r} v'(x)^2 dx = \frac{N_{cr}\pi^2 c^2 e^{-m} m \sinh(m)}{4 l_r} \tag{14}$$

Using Eq. (A.2), the following expression for the buckling load is obtained:

$$N_{cr} = \frac{c_h {l_r}^4 + \left(5 + 6\pi^2 + \pi^4\right) EIm^4}{\left(1 + \pi^2\right) {l_r}^2 m^2} \tag{15}$$

From the minimization of Eq. (15), the value of m corresponding to the first critical load reads

$$m_{min} = \left(\frac{c_h}{EI}\right)^{1/4} \frac{l_r}{\left(5 + 6\pi^2 + \pi^4\right)^{1/4}} \tag{16}$$

By substitution into Eq. (15), the expression for the first buckling load N_p proposed in this paper is

$$N_p = 2\sqrt{c_h EI}\frac{\sqrt{5 + 6\pi^2 + \pi^4}}{1 + \pi^2} \approx 1.17 N_{ki} \tag{17}$$

Interestingly, N_p is 1.17 times the critical load N_{ki} obtained with the classical formulation. This result will be validated in the next section using FE analyses, showing that N_{ki} underestimates the critical load by on average 22%, while N_p provides a highly accurate prediction.

It is worth noting that m should be a natural number. However, in a general case the solution of Eq. (16) gives a real number. Nevertheless, as explained in Appendix A.1, this does not affect the solution sensibly and the estimation of the critical buckling load is accurate.

5. FE analyses

The authors developed a monodimensional FE model of the screw in Abaqus. Initially, the model is used for validating the expressions for the theoretical buckling loads derived in the previous section. In a second step, the authors modified the model to include the effects of initial geometric imperfection, calibrated on the experimental data.

5.1. Model description and methodology

Two different finite element models have been developed. The first model is defined to validate the analytical formulations for the instability of screws, whilst the latter aims at describing the system's non-linear behaviour until failure.

In the linear buckling model (LBM) shown in Fig. 7(a), shear-deformable beam elements with linear interpolation represent the screw. The screw section is assumed as solid

circular of diameter $d = 1.1d_1$. A linear elastic constitutive model is adopted for steel ($E = 210000$ N/mm^2). Two orders of elastic spring elements describe the screw-timber interaction in the axial and transversal directions. Axial and transversal connectors stiffness are assumed as $C_v = c_v l_m$, and $C_h = c_h l_m$ respectively, where l_m is the length of the beam element between two adjoining connectors and c_v and c_h are determined according to Eq. (A.12) and Eq. (7), respectively. The screw-head is assumed free to rotate and to translate in the screw axial direction while the transversal displacement is restrained. The load $\bar{F}$ is applied as a concentrated force to the head-side end node. The eigenvalues analysis is conducted in the initial undeformed and imperfection-free geometry. Differently from Bejtka [1], the screw head is considered pinned. The effects of different restraints at the screw heads are discussed in Appendix C.

The non-linear static incremental model (NLSIM) in Fig. 7(b) assumes an elastic-plastic constitutive law for the steel, whilst an elastic behaviour is considered for both axial and transversal springs. In this way, the model can only predict the screw bending failure mode while neglecting the push-in failure mode, which is outside this research's scope. An imposed displacement $\bar{u}$ is applied to the head-side end node. A static-incremental geometrically and mechanically non-linear analysis is carried out on a defected screw geometry. As the initial screw geometrical imperfection shapes, the first buckling mode from LBM has been adopted (Fig. 7(b)) [65]. The amplitude A_{imp} is calibrated on the experimental results.

5.2. Theoretical buckling validation

The formulation in Eq. (17) is validated against the theoretical buckling loads obtained from the FE model. Tab. 6 compares the theoretical buckling load estimated with the LBM ($N_{fem,buck}$) with N_{ki} in Eq. (6) and N_p in Eq. (17).

The experimental capacities (F_{exp}) cannot be reference values for validating the accuracy of the theoretical buckling load predictions and are not reported in Tab. 6. The reference values, assumed as ideal buckling loads, are the FE predictions in $N_{fem,buck}$. Despite the straightforwardness of the proposed formulation, the mean error associated with N_p in Eq. (17) is approximately 9%. Conversely, the mean error of N_{ki} is approximately 22%. It must be remarked that the error associated with N_{ki} can be considered reasonable

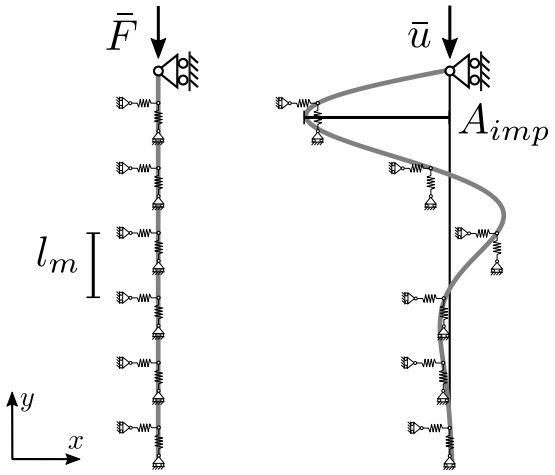

Figure 7: Finite element models: (a) Linear buckling analysis and (b) Non-linear static incremental analysis.

Table 6: Validation of the theoretical buckling load estimated with the FE model ($N_{fem,buck}$), compared against the theoretical buckling loads corresponding to the Winkler beam (N_{ki}) in Eq. (6) and the proposed Eq. (17) (N_p). The input parameters are $\rho = 430$ kg/m^3, α=90°, $d_1 = 0.65d$, E=210 GPa. The diameter assumed in the calculations is $1.1d_1$.

Label	l_r [mm]	d_1 [mm]	c_h [MPa]	c_v [Mpa]	N_{ki} [kN]	N_p [kN]	$N_{fem,buck}$ [kN]
VGZ	160.0	5.0	117.8	55.3	55.2	64.6	73.0
WT-T	130.0	5.9	124.0	64.6	77.7	90.9	109.7
HT-T	160.0	5.7	123.0	56.8	73.7	86.2	99.5
HT-T	180.0	5.7	123.0	52.9	73.7	86.2	97.3
HT-T	200.0	5.7	123.0	49.6	73.7	86.2	95.6
HT-T	200.0	5.7	123.0	49.6	73.7	86.2	90.6
HT-T	300.0	5.7	123.0	38.9	73.7	86.2	89.4
VGZ	440.0	6.4	128.1	31.7	95.2	111.3	113.7
				Relative error	-0.22	-0.09	

in some applications (like geotechnics), where the uncertainty of the soil properties are far more relevant than the modelling assumptions in Eq. (6). However, the high accuracy and elegance of Eq. (17) endorse its use in place of N_{ki} for predicting the ideal buckling of the screws, where c_h can be estimated with reasonable accuracy. Rarely, in mechanics, high accuracy can be achieved with straightforward analytical formulations.

5.3. Calibration of the geometric defects

Initial imperfections and second-order effects affect the failure load of a compressed beam on an elastic medium. The capacity of a perfectly straight beam made of an elastic-plastic material is equal to its plastic axial force $N_{pl} = f_y \pi d^2/4$. When initial imperfections occur, a bending moment arises in the beam as the beam deforms. Accordingly, the

eccentricity between the load and the beam axis increases. The failure of the systems occurs for a combination of axial force and bending moment. Therefore the yielding tensile stress f_y and the initial imperfection amplitude A_{imp} directly influences the ultimate compression load of the screw. However, the failed configuration corresponds to the buckling mode, as occurs in all instability phenomena [65]. For this reason, it is necessary to know the ideal instability phenomena.

In the NLSIM, f_y is equal to the mean value of the tensile failure stress of the tested screws ($f_y = 1200$ N/mm^2). At the same time, the imperfection amplitude is calibrated on experimental results. The imperfection amplitude A_{imp} is defined as a fraction of the screw length following the general approach for steel structures [63]:

$$A_{imp} = l/\xi \tag{18}$$

The value of ξ has been determined by minimizing the sum of the squared relative error between NLSIM and the experimental results of the configurations that exhibited bending failure mode (Fig. 6):

$$S = \sum_{n=3}^{8} \left(\frac{F_{fem,\mathrm{NLSIM}} - F_{exp}}{F_{exp}} \right)^2 \tag{19}$$

Fig. 8 shows the NLSIM failure load for increasing eccentricity values. The value of the objective function S is minimized when $\xi = 500$. The plot in Fig. 8 highlights the significant role of the geometric imperfections. In the case of low imperfections, the predicted capacity almost corresponds to the plastic capacity in Eq. (5). An increasing value of the imperfection significantly reduces the axial capacity and exalts the effects of instability. In the tested configurations, the estimated imperfection, equal to l/500, is very low compared to steel structures where the lowest imperfection class a_0 almost corresponds to an eccentricity equal to l/350 [63]. However, the two scenarios, the screw and the compressed steel member, are not comparable due to the mentioned differences in the buckling modes. Therefore, as discussed in the previous sections, the screws deserve a dedicated calibration of the imperfection coefficients in Eq. (3) and Tab. 3.

Fig. 8(b) displays the force-displacement curves of the updated model with $A_{imp} = l/500$, while the deformed shapes at failure and the bending moment contour are displayed

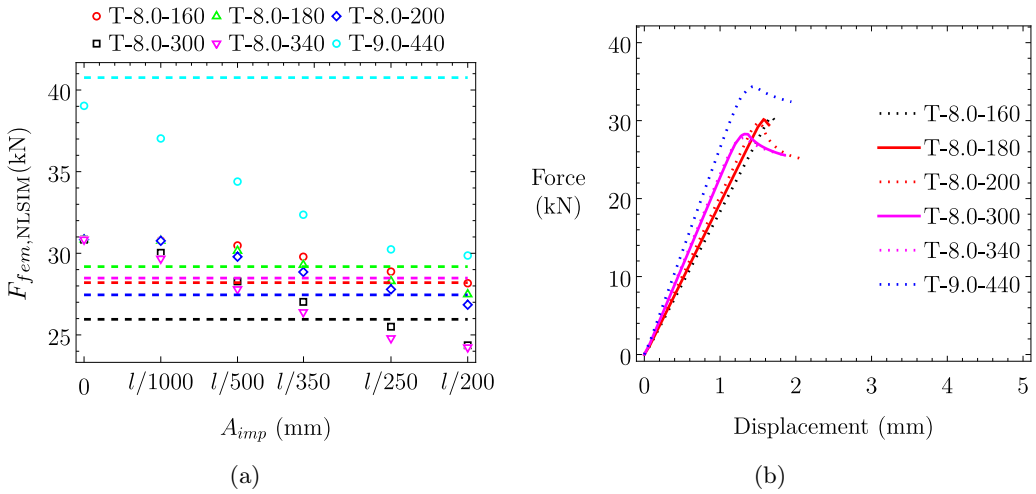

Figure 8: (a) Finite element predicted failure loads (markers) and experimental failure loads (dashed lines) for varying imperfection amplitude. (b) Finite element force-displacement curves with $A_{imp} = l/500$.

Table 7: Finite element model (NLSIM) vs experimental results VS experimental results. The input parameters are $\rho = 430$, $f_y = 1200$, α=90°, $d_1 = 0.65d$, E=210 GPa and $A_{imp} = l/500$. The diameter assumed in the calculations is $1.1d_1$.

Configuration	$F_{fem,\mathrm{NLSIM}}$ [kN]	F_{exp} [kN]	Relative error [%]
T-7.0-160	23.3	21.9	6.4
T-8.2-160	32.3	21.3	51.9
T-8.0-160	30.7	28.2	9.0
T-8.0-180	30.5	29.2	4.6
T-8.0-200	30.3	27.5	10.4
T-8.0-300	29.2	26.0	12.5
T-8.0-340	28.8	28.5	1.2
T-9.0-440	35.9	40.8	-11.8

in Fig. 8. Tab. 7 compares the experimental vs FE estimations of the capacity using the optimized value for A_{imp} equal to l/500. The relative error is minimum and generally less than 10% except for the screw T-8.2-160.

It is worth noting that the bending moment maxima approximately manifest at the same distance from the screw head for all configurations ($\approx 15 - 20$ mm). This result is confirmed by the experimental evidence in Fig. 6. The obtained value for the imperfection coefficient could be considered low due to the carefulness carried out in the screw drilling using a template for a right-angle insertion. Additionally, as shown in Fig. 6, there were no defects which could have deviated the screw during the drilling, thus causing a straightness defect.

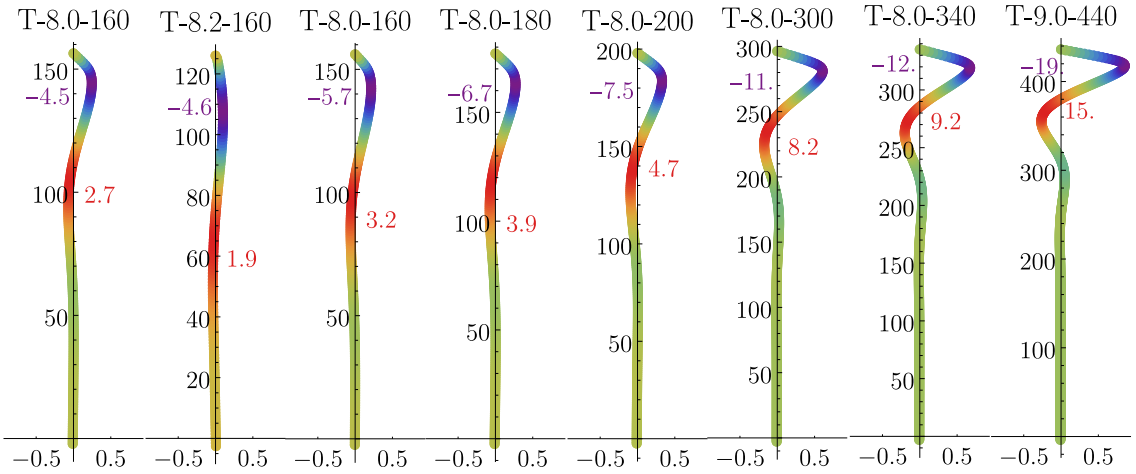

Figure 9: Finite element predicted deformed shape at failure and bending moment contour ($kN \cdot mm$).

6. Monte Carlo simulations and imperfection coefficient calibration

The experimental results and analytical findings suggest two improvements to the model in Eq. (21):

- Replacing N_{ki} with N_p in Eq. (17).
- Adopting an imperfection coefficient (α_g) calibrated for different values of the geometric uncertainty (A_{imp}). This value depends on the laminated timber product, the distribution of defects, and the human error in screw insertion. This value should be decided on a case-by-case basis.

The authors carried out a Markov chain Monte Carlo analysis [61] to simulate the capacity of the screws with various lengths and diameters, assuming the uncertainty of the material inputs, as reported in Tab. 8. The diameter (d) has been randomly sampled from

Table 8: Input parameters of the Monte Carlo simulations.

Symbol	Distribution	Characteristics	
d [mm]	Uniform	Lower Bound=1	Upper Bound=20
l_r [mm]	$l = [\pi(d/2)^2 f_y]/(f_{ax} d)$		
ρ [kg/m^3]	Normal	μ=470	CoV=0.1 [52]
E [GPa]	Normal	μ=210	CoV=0.05 [52, 66–68]
f_y [MPa]	Normal	μ=1200	CoV=0.05 [52, 66, 67]
f_w [MPa]	Normal	μ=15	CoV=0.1 [52]
c_h [MPa]	Eq. (7) $+\sigma_h \epsilon$	σ_h=19.58	$\epsilon \propto \mathcal{N}(0,1)$ [1]
c_v [MPa]	Eq. (A.12) $+\sigma_v \epsilon$	σ_v=14.86	$\epsilon \propto \mathcal{N}(0,1)$[1]

a uniform distribution with bounds in Tab. 8. The threaded length of the screw was obtained by inverting the equation for the withdrawal resistance, assuming the withdrawal

resistance was normally distributed. Likewise, the yielding strength and the wood density are normally distributed following [52, 66, 67]. The scientific literature does not report the uncertainties associated with the empirical regressions for c_h and c_v. Bejtka only reports the coefficient of determination of the fitting for c_h and c_v. Therefore, the authors digitally converted the regression plots in the doctoral thesis from Bejtka [1] to estimate the fitting error. The histogram plot of the error follows a normal distribution with nearly-zero mean and variances reported in Tab. 8. Therefore, the authors included the uncertainty of c_h and c_v from a random sampling of the standard normal distribution (ϵ).

The authors repeated the MCMC for four values of imperfection: l/500, l/400, l/300, l/200, l/100 and l/50. Fig. 10 shows the histogram plots of the sampled values for f_y,

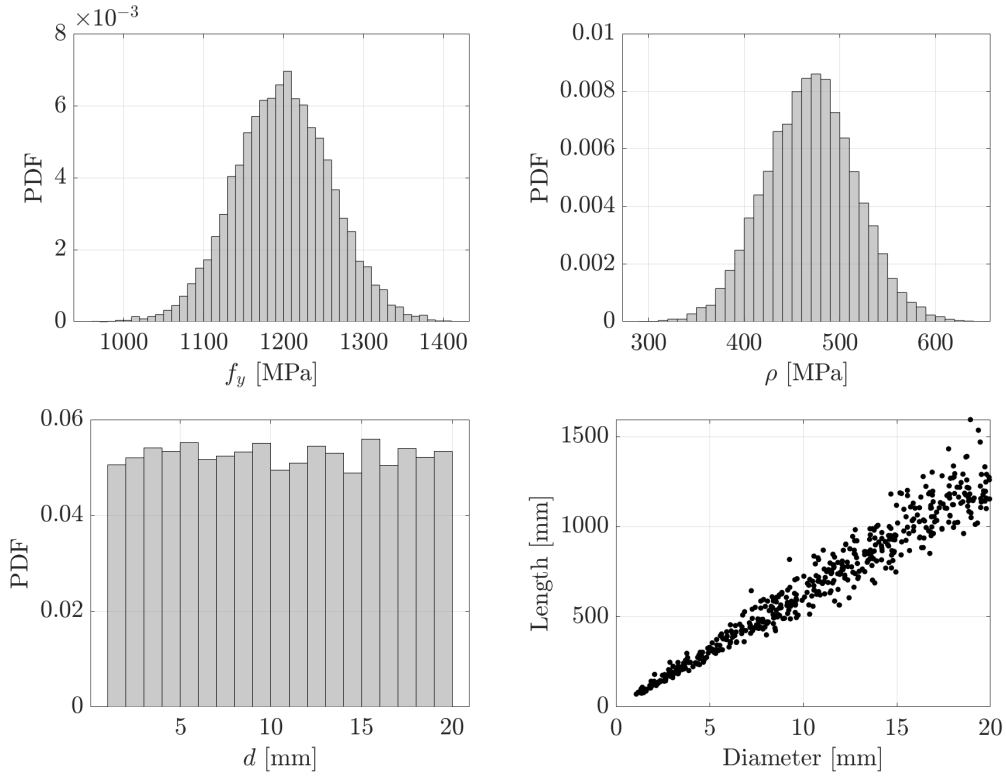

Figure 10: Plots of the realization of the input parameters for the Monte Carlo analyses: (a) yielding strength, (b) wood density, (c) diameter, (d) threaded length of the screw.

ρ, d and the threaded length of the screw. Fig. 11 shows the superposition between the deterministic estimations of c_h and c_v and the ones with uncertainty based on Tab. 8. The c_h and c_v realizations have overlapped with the results reported by Bejtka for further validation of the proposed approach. The scatter of the data is very close to the one in the plots of Bejtka. The convergence of the Monte Carlo simulations was checked a posteriori

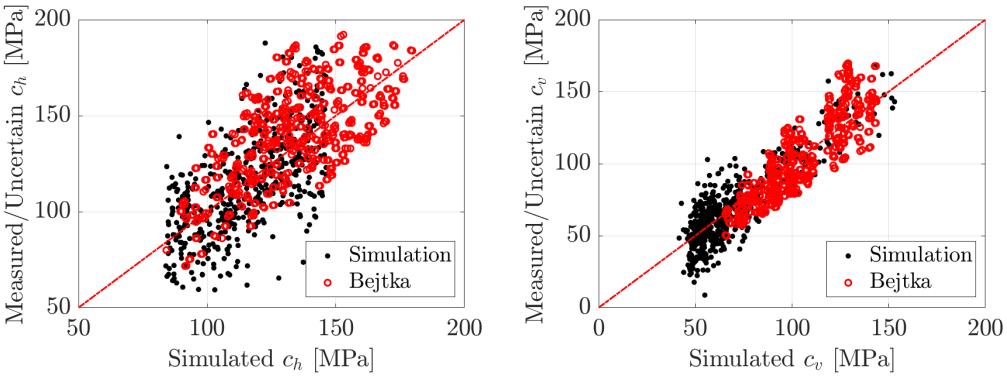

Figure 11: In black the experimental/simulated values of c_h and c_v using the inputs in Tab. 8 vs the deterministic predictions using Eq. (7) and Eq. (A.12), respectively. In red the experimental vs predicted values from Bejtka [1].

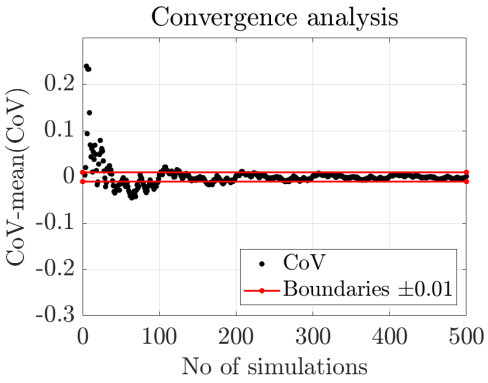

Figure 12: Convergence of the Monte Carlo analyses in terms of Coefficient of covariance (CoV).

from the CoV of the axial capacity. The analyses were stopped at 500 simulations since the variation of the CoV was less than 1%, as shown in Fig. 12. The values of α_g for the different geometric defects are obtained by minimizing the following objective function:

$$\hat{\alpha}_g = \arg\min_{\alpha_g \in \Omega} \left\{ [F_c - F_{fem,\mathrm{NLSIM}}(A_{imp})]^2 \right\} \tag{20}$$

where $\Omega \in \mathrm{R}$, F_c is the buckling model in Eq. (1) where Eq. (17) is used for assessing the ideal buckling force and α_g in Eq. (3) is unknown. At the same time, $F_{fem,\mathrm{NLSIM}}$ is the capacity predicted by the FE model function of the initial geometric imperfection (A_{imp}).

Tab. 9 reports the values of the obtained imperfection coefficients by minimizing Eq. (20) using N_p for the ideal buckling load.

As expected, an increment of the imperfection level determines an increment of the corresponding imperfection coefficient α_g, see the stability curves in Fig. 13.

Fig. 14(a) shows the FE predictions of the theoretical buckling load vs the estimations

Table 9: Values of the calibrated imperfection coefficient $\hat{\alpha_g}$ as a function of the initial imperfection expressed as a fraction of the screw length. The ideal buckling load is estimated with Eq. (17).

$\hat{\alpha}_g$	l/500	l/400	l/300	l/200	l/100
	0.16	0.21	0.27	0.34	0.72

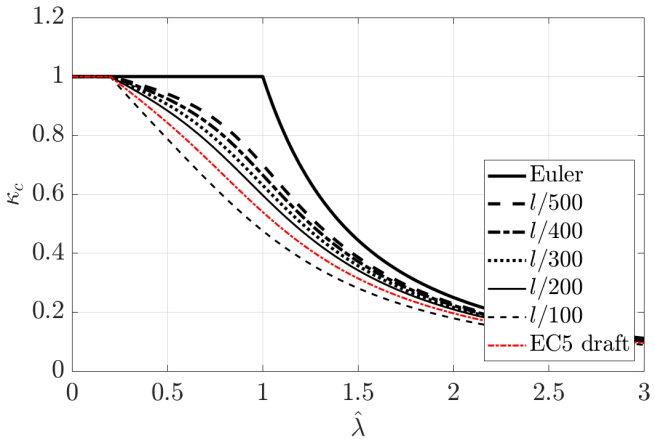

Figure 13: Stability curves based obtained with the imperfection coefficients in Tab. 3.

using Eq. (6) (N_{ki}) and Eq. (17) (N_p). Additionally, Fig. 14(a) displays the FE predictions of the axial capacity vs the estimations of Eq. (5) with N_p and the imperfection coefficients in Tab. 9. Tab. 10 reports the error of the three models F_c, N_p and N_{ki} in terms of mean error, standard deviation (SD), mean squared error (MSE), maximum Absolute Error (MAE), root Mean Squared Error (RMSE), and coefficient of determination (R^2), considering all defect scenarios.

Table 10: Mean error, standard deviation (SD) and mean squared error (MSE), Maximum Absolute Error (MAE), Root Mean Squared Error (RMSE) or the difference between the FE and analytically predicted force values (F_c), shown in Fig. 14. R^2 is the coefficient of determination of the fitting.

Model	Mean	SD	MSE	R^2	MAE	RMSE
F_c	-0.56	4.15	17.34	0.95	15.36	4.16
N_p	13.71	28.48	991.19	0.60	127.71	31.48
N_{ki}	-20.73	27.94	1202.71	0.56	114.30	34.68

The main findings of the analyses can be grouped into the following considerations:

- The theoretical buckling model which best fits the FE buckling predictions is the one in Eq. (17), despite the considered uncertainties have a significant effect on the error metrics in Tab. 10. The differences between the predictions with N_p or N_{ki} are not significant in the presence of uncertainty. However, given the better performance of N_p and the more solid mechanical background, N_p should be preferred to N_{ki}.

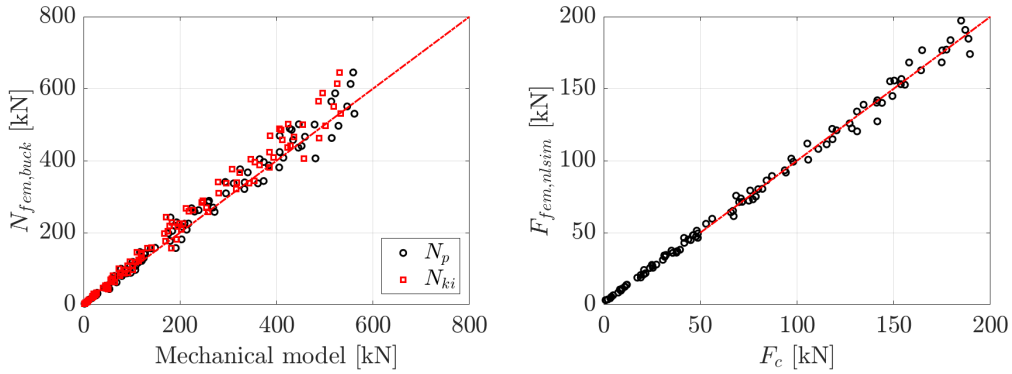

Figure 14: (a) FE predictions of the theoretical buckling load vs the estimations using Eq. (6), and Eq. (17). (b) FE predictions of the axial capacity using N_p in Eq. (17) and the imperfection coefficients in Tab.3.

- The axial capacity models obtained using Eq. (17) (N_p) and the imperfection coefficients in Tab. 10 are excellent. Therefore, despite the considered uncertainties of the FE model, the deterministic assessment of the capacity using the averaged values for the parameters in Tab. 8 is extremely accurate, with excellent error metrics in all configurations.

In conclusion, the prediction of the axial capacity of the screw in case of buckling can be carried out using Eq. (17) (N_p), where α_g is taken from Tab. 3. The main limitation of this paper is the lack of an extended experimental campaign relating the effects of geometric defects of the screw to the screw itself, the laminated timber product, the strength class (the density of defects), the timber species, etc. Therefore, future research efforts will aim at quantifying the influence of defects on the capacity estimate of the screws from experimental investigations.

Design codes require estimating the characteristic value, which can be obtained by replacing all mean values involved in the computation with the characteristic ones corresponding to a 5% fractile. Additionally, the potential use of the formulation requires the definition of an uncertainty factor γ_M to avoid underestimating the capacity due to the uncertainties involved. The code-format design capacity in Eq. (21) can be written as

$$F_{c,k} = \frac{1}{\gamma_M} k_c N_{pl,k} \text{ where } \gamma_M = 1.18 \tag{21}$$

The uncertainty factor γ_M is estimated by assuming that the design value is less than the

corresponding experimental value with a probability equal to p as

$$P\left[F_c < F_{fem,\mathrm{NLSIM}}\right] = p \tag{22}$$

where F_c and F_{fem} are the simulated and experimental capacity corresponding to 1% deformation respectively, and p depends on the assumed reliability threshold. The European building code sets p as $\Phi(\alpha_R \beta_{LS})$, where $\Phi(\cdot)$ is the standard Normal cumulative distribution function, α_R is the sensitivity factor for the capacity, and β_{LS} is the safety index relevant to the considered limit state. Assuming a 50-years reference period for serviceability limit states (see Tab. C2 in Eurocode 0), $\beta_{LS} = 1.5$. The obtained γ_M coefficients corresponding to $\beta = 1.5$ are reported in Tab. 11 as a function of the defect level. The

Table 11: Values of the estimated uncertainty factors (γ_M) as a function of the initial imperfection expressed as a fraction of the screw length.

γ_M	l/500	l/400	l/300	l/200	l/100
	1.2	1.2	1.2	1.3	1.3

authors did not provide a unique value for the uncertainty factor, valid for all levels of defects. An increased defect causes a slight worsening of the predictions based on the framework in Tab. 2. Therefore, the uncertainty factors increase from an l/500 to an l/100 defect amplitude.

7. Conclusions

This paper proposes a novel buckling model for timber screws based on the general mathematical framework for the instability of compressed steel members. The main shortcomings of the existing buckling model for the screws enclosed in the current Eurocode 5 draft are two: (1) the ideal buckling load is underestimated due to an incorrect assumption on the buckling shape; (2) the imperfection coefficients valid for compressed steel members exhibiting a sine-like buckling mode cannot be considered valid for timber screws loaded at one end.

The experimental and FE investigations showed that the buckling mode of the screws loaded at their heads resembles a damped sine function. As a result, the deformation of a buckled screw is concentrated at the load application point, while the remaining part of

the screw is almost undeformed. Based on this evidence, the authors derived the critical buckling load of the screws assuming a deformation field having the shape of the observed failure modes. The error of the obtained formulation validated against the FE predictions is approximately equal to 9%. The proposed formulation is concise and corresponds to the classical one for the instability of Winkler beams multiplied by 1.17.

The proposed equation for the ideal buckling is used for calibrating the imperfection coefficients assuming the uncertainty of the mechanical parameters from suitable probability distributions and increasing levels of geometric imperfections of the screws. The authors estimated the capacity of multiple screw realizations following a Markov chain Monte Carlo approach. The axial capacity of the screw is obtained from nonlinear FE push-in simulations assuming an initial screw geometry corresponding to the first buckling mode with maximum amplitude expressed as a fraction of the screw length. The simulated data are used to calibrate the imperfection coefficients for several defect amplitudes. Additionally, the authors estimated the uncertainty factor of the corresponding design equation for possible standard implementation.

8. Data availability statement

All data, models and codes supporting this study's findings are available from the corresponding author upon reasonable request.

9. Acknowledgment

The authors acknowledge Mathias Bech (Rothoblaas), Harald Liven (Moelven) and Peter Engström-Øren (SFS) for providing the material. Roar Økseter, Scott Brenna, Frode Anker Røsstad (NMBU) and the master thesis students Eldbjørg Aaraas Hånde and Kari Ryen Thunberg are kindly acknowledged for their support during the experimental campaign.

References

[1] I. Bejtka, *Verstärkung von bauteilen aus holz mit vollgewindeschrauben.* KIT Scientific Publishing, 2005.

[2] M. Piazza, R. Modena, and R. Tomasi, *Strutture in legno. Materiale, calcolo e progetto secondo le nuove normative europee.* Hoepli Editore, 2005.

[3] G. Pirnbacher and G. Schickhofer, "Schrauben im vergleich-eine empirische betrachtung," *6. GraHFT'07*, 2007. cited By 6.

[4] P. Dietsch and R. Brandner, "Self-tapping screws and threaded rods as reinforcement for structural timber elements–a state-of-the-art report," *Construction and Building Materials*, vol. 97, pp. 78–89, 2015.

[5] F. Colling, "Holzbau-grundlagen und bemessungshilfen. 2. auflage," *Holzbau-Grundlagen und Bemessungshilfen*, 2008.

[6] H. Brüninghoff, C. Schmidt, and T. Wiegand, "Praxisnahe empfehlungen zur reduzierung von querzugrissen bei geleimten satteldachbindern aus brettschichtholz," *Bauen Mit Holz*, vol. 95, no. 11, pp. 928–937, 1993.

[7] F. Boggian, A. Aloisio, and R. Tomasi, "Experimental and analytical study of friction connection for seismic retrofit with cross-laminated timber (clt) panels," *Earthquake Engineering & Structural Dynamics*, vol. 51, no. 14, pp. 3304–3326, 2022.

[8] K. Möhler and W. Siebert, "Untersuchungen zur erhöhung der querzugfestigkeit in gefährdeten bereichen," *Bauen Mit Holz*, vol. 86, no. 6, pp. 388–393, 1984.

[9] H. Kreuzinger, "Holzbau," *Handbuch für Bauingenieure*, 2002.

[10] R. Tomasi, A. Crosatti, and M. Piazza, "Theoretical and experimental analysis of timber-to-timber joints connected with inclined screws," *Construction and building materials*, vol. 24, no. 9, pp. 1560–1571, 2010.

[11] R. Tomasi, A. Aloisio, E. A. Hånde, K. R. Thunberg, and E. Ussher, "Experimental investigation on screw reinforcement of timber members under compression perpendicular to the grain," *Engineering Structures*, vol. 275, p. 115163, 2023.

[12] G. Schiro, I. Giongo, W. Sebastian, D. Riccadonna, and M. Piazza, "Testing of timber-to-timber screw-connections in hybrid configurations," *Construction and Building Materials*, vol. 171, pp. 170–186, 2018.

[13] H. Kreuzinger, "Platten, scheiben und schalen - ein berechnungsmodell für gängige statikprogramme," *Bauen Mit Holz*, vol. 1, no. 1, pp. 34–39, 1999.

[14] H. Kreuzinger, "Verbundkonstruktionen," *Holzbaukalender 2002*, pp. 598–621, 2001.

[15] D. E. . 1-1/NA *Norwegian National Annex - Nationally Determined Parameters - Eurocode 5: Design of Timber Structures - Part 1-1: General - Common Rules and Rules for Buildings*, 2010.

[16] S. Aicher and L. Höfflin, "Glulam beams with round holes-a comparison of different design approaches vs. test data, cib-w18/35-12-1," *Proceedings of the International Council for Research and Innovation in Building and Construction, Working Commission W18-timber Structures*, 2002.

[17] S. Aicher and L. Höfflin, "Design of rectangular holes in glulam beams," *Otto-Graf-J.*, vol. 14, pp. 211–229, 2003.

[18] H. Kolb and A. Epple *Verstärkungen von Durchbrochenen Brettschichtholzbindern, Schlussbericht Zum*

Forschungsvorhaben I.4-34810, 1985.

[19] S. Aicher, L. Höfflin, and H.-W. Reinhardt, "Round holes in members made of glued laminated timber. part 2: Load capacity and design [runde durchbrüche in biegeträgern aus brettschichtholz teil 2: Tragfähigkeit und bemessung]," *Bautechnik*, vol. 84, no. 12, pp. 867–880, 2007.

[20] S. Aicher and L. Höfflin, "Glulam beams with holes reinforced by steel bars," *Glulam beams with holes reinforced with steel bars*, 2009.

[21] S. Aicher, "Glulam beams with internally and externally reinforced holes - test, detailing and design," *International Council for Research and Innovation in Building and Construction, Working Commission W18 - Timber Structures, Alghero, Italy*, pp. 1–13, 2011.

[22] P. Dietsch, S. Rodemeier, and H. Blaß, "Transmission of perpendicular to grain forces using self-tapping screws," in *International Network on Timber Engineering Research INTER, Meeting 6*, 2019.

[23] I. Bejtka and J. Blaß H. ., "Self-tapping screws as reinforcements in connections with dowel-type fasteners, cib-w18/38-7-4," *Proceedings of the International Council for Research and Innovation in Building and Construction, Working Commission W18-timber Structures, Meeting 38, Karlsruhe, Germany*, 2005.

[24] I. Bejtka and J. Blaß H. ., "Self-tapping screws as reinforcements in beam supports, cib-w18/39-7-2," *Proceedings of the International Council for Research and Innovation in Building and Construction, Working Commission W18-timber Structures, Meeting 39, Florence, Italy*, 2006.

[25] H. Blass and G. Steck, "Querzugverstärkungen von holzbauteilen: Teil 1 - teil 3," *Querzugverstärkungen Von Holzbauteilen: Teil 1–Teil 3*, vol. 101, no. 3, pp. 42–46, 1999.

[26] H. Blass and I. Bejtka *Querzugverstärkungen in Gefährdeten Bereichen mit Selbstbohrenden Holzschrauben (in German)*, 2003.

[27] F. Kollmann and W. Côté *Principles of Wood Science and Technology*, 1968. cited By 1537.

[28] O. Graf, "Beobachtungen über den einfluss der größe der belastungsfläche auf die widerstandsfähigkeit von bauholz gegen druckbelastung quer zur faser," *Der Bauingenieur*, vol. 18, pp. 498–501, 1921.

[29] E. Suenson, "Zulässiger druck auf querholz," *Holz als Roh- und Werkstoff: European Journal of Wood and Wood Industries*, vol. 1, no. 6, pp. 213–216, 1938.

[30] E. Gehri, "Timber in compression perpendicular to grain, in iufro," *Copenhagen*, 1997.

[31] U. Hübner, "Mechanische kenngröben von buchen-, eschen- und robinienholz für lastabtragende bauteile," *Mechanische Kenngröben von Buchen-, Eschen- und Robinienholz für Lastabtragende Bauteile*, 2013.

[32] E. Gaber, "Druckversuche quer zur faser an nadel- und laubhölzern," *Holz als Roh- und Werkstoff*, vol. 3, no. 7-8, pp. 222–226, 1940.

[33] A. Frey-Wyssling Stüssi, "Festigkeit und vervormung von nadelholz bei druck quer zur faser," *Scheiz Z. Forstwes.*, vol. 3, pp. 106–114, 1948.

[34] A. Rothmund *Über Die Wiederstandsfähigkeit des Holzes Gegen Druck Quer Zur Faser*, 1949.

[35] P. Hoffmeyer, L. Damkilde, and T. Pedersen, "Structural timber and glulam in compression perpendicular to grain," *Holz als Roh - und Werkstoff*, vol. 58, no. 1-2, pp. 73–80, 2000.

[36] A. Leijten, "The bearing strength capacity perpendicular to grain of norway spruce–evaluation of three structural timber design models," *Construction and Building Materials*, vol. 105, pp. 528–535, 2016.

[37] T. van der Put, "Tension perpendicular to the grain at notches and joints," *Tension Perpendicular at Notches and Joints*, 1990.

[38] B. Standard, "Eurocode 3—design of steel structures—," *BS EN 1993-1*, vol. 1, p. 2005, 2006.

[39] H. G. Poulos, E. H. Davis, *et al.*, *Pile foundation analysis and design*, vol. 397. Wiley New York, 1980.

[40] H. Granholm, *On the elastic stability of piles surrounded by a supporting medium*, vol. 89. Svenska Bokhandelscentralen A.-B, 1929.

[41] M. Hetenyi *Beams on Elastic Foundation*, 1946. cited By 1456.

[42] M. Eisenberger and D. Yankelevsky, "Exact stiffness matrix for beams on elastic foundation," *Computers and Structures*, vol. 21, no. 6, pp. 1355–1359, 1985. cited By 78.

[43] R. West and M. Pavlović, "A fast iterative algorithm for eigenvalue determination," *Computers and Structures*, vol. 63, no. 4, pp. 749–758, 1997.

[44] S. P. Timoshenko and J. M. Gere, "Theory of elastic systems," 1961.

[45] K. Terzaghi, "Evaluation of coefficients of subgrade reaction," *Geotechnique*, vol. 5, no. 4, pp. 297–326, 1955. cited By 517.

[46] *Design of Laterally Loaded Piles*, vol. 103, 1984. cited By 1.

[47] R. West *Modal Clustering in the Vibration of Beams Partially Embedded in a Winkler Foundation*, 1991. cited By 5.

[48] M. Pavlović and S. Tsikkos, "Beams on quasi-winkler foundations," *Engineering Structures*, vol. 4, no. 2, pp. 113–118, 1982. cited By 16.

[49] R. Cucuzza, G. Devillanova, A. Aloisio, M. M. Rosso, and G. C. Marano, "Analytical solutions for piles' lateral deformations: The nonlinear stiffness case," *International Journal of Mechanical Sciences*, vol. 229, p. 107505, 2022.

[50] M. E. Heelis, R. P. West, *et al.*, "The stability of uniform-friction piles inhomogeneous and non-homogeneous elastic foundations," *International journal of solids and structures*, vol. 36, no. 22, pp. 3277–3292, 1999.

[51] A. D. Kerr, "On the buckling of slender piles," *Soils and foundations*, vol. 28, no. 2, pp. 144–148, 1988.

[52] H. J. Blaß, I. Bejtka, and T. Uibel, *Tragfähigkeit von Verbindungen mit selbstbohrenden Holzschrauben mit Vollgewinde*, vol. 4. 2006.

[53] A. Ringhofer, M. Grabner, R. Brandner, and G. Schickhofer, "Sgsc 3.2.1-1-prüftechnische ermittlung des tragverhaltens der einzelschraube in der bsp-schmalfläche," *Internal Research Report, Holz.bau Forschungs Gmbh, Institute of Timber Engineering and Wood Technology*, 2013.

[54] H. Stamatopoulos and K. A. Malo, "On strength and stiffness of screwed-in threaded rods embedded in softwood," *Construction and Building Materials*, vol. 261, p. 119999, 2020.

[55] J. Ehlbeck, R. Görlacher, and H. Werner, "Determination of perpendicular-to-the-grain tensile stresses

in joints with dowel-type-fasteners," *Proceedings of CIB-W18*, 1989.

[56] H. Kolb and P. Frech, "Untersuchungen an durchbrochenen bindern aus brettschichtholz [untersuchungen an durchbrochenen bindern aus brettschichtholz]," *Holz als Roh- und Werkstoff: European Journal of Wood and Wood Industries*, vol. 35, no. 4, pp. 125–134, 1977.

[57] "Eurocode 5. design of timber structures. bridges," *Eurocode 5: Design of Timber Structures - Part 1-1: General - Common Rules and Rules for Buildings*, 2004. cited By 841.

[58] Y. De Santis and M. Fragiacomo, "Timber-to-timber and steel-to-timber screw connections: Derivation of the slip modulus via beam on elastic foundation model," *Engineering Structures*, vol. 244, p. 112798, 2021.

[59] M. A. H. Mirdad, A. Jucutan, R. Khan, J. Niederwestberg, and Y. H. Chui, "Embedment and withdrawal stiffness predictions of self-tapping screws in timber," *Construction and Building Materials*, vol. 345, p. 128394, 2022.

[60] R. Jockwer, A. Frangi, R. Steiger, and E. Serrano, "Enhanced design approach for reinforced notched beams, cib-w18/46-6-1," *Proceedings of the International Council for Research and Innovation in Building and Construction, Working Commission W18-timber Structures*, 2013.

[61] C. P. Robert and G. Casella, *Monte Carlo statistical methods*, vol. 2. Springer, 1999.

[62] H. M. Kattan, "Those who fail to learn from history are doomed to repeat it. agile processes in software engineering and extreme programming: poster presented in the 18th international conference on agile software development, xp 2017. held in cologne, germany," 2017.

[63] G. Ballio and F. M. Mazzolani, *Theory and design of steel structures*. Taylor & Francis, 1983.

[64] O. Belluzzi, *Scienza delle Costruzioni, vol. 4*. Zanichelli, 1982.

[65] D. Bigoni, *Nonlinear solid mechanics: bifurcation theory and material instability*. Cambridge University Press, 2012.

[66] A. Ringhofer, M. Augustin, and G. Schickhofer, "Basic steel properties of self-tapping timber screws exposed to cyclic axial loading," *Construction and Building Materials*, vol. 211, pp. 207–216, 2019.

[67] P. Niebuhr and M. Sieder, "High-cycle fatigue behavior of a self-tapping timber screw under axial tensile loading," *Journal of Failure Analysis and Prevention*, vol. 20, pp. 580–589, 4 2020.

[68] A. Y. Al-Attraqchi, M. J. Hashemi, and R. Al-Mahaidi, "Hybrid simulation of bridges constructed with concrete-filled steel tube columns subjected to horizontal and vertical ground motions," *Bulletin of Earthquake Engineering*, vol. 18, no. 9, pp. 4453–4480, 2020.

[69] N. Tullini, A. Tralli, and D. Baraldi, "Stability of slender beams and frames resting on 2D elastic half-space," *Archive of Applied Mechanics*, vol. 83, no. 3, pp. 467–482, 2013.

[70] N. Tullini, A. Tralli, and D. Baraldi, "Buckling of Timoshenko beams in frictionless contact with an elastic half-plane," *Journal of Engineering Mechanics*, vol. 139, no. 7, pp. 824–831, 2013.

[71] F. O. Falope, L. Lanzoni, and E. Radi, "Buckling of a Timoshenko beam bonded to an elastic half-plane: Effects of sharp and smooth beam edges," *International Journal of Solids and Structures*, vol. 185, pp. 222–239, 2020.

[72] M. Eisenberger, "Buckling loads for variable cross-section members with variable axial forces," *Inter-*

national Journal of Solids and Structures, vol. 27, no. 2, pp. 135–143, 1991.

[73] D. Hui, "Postbuckling behavior of infinite beams on elastic foundations using Koiter's improved theory," *International journal of non-linear mechanics*, vol. 23, no. 2, pp. 113–123, 1988.

Appendix A. Discussion on the approximations in N_{ki}

In the following, we discuss the limitations of of the buckling formulations for N_{ki}, as highlighted in the section dealing with the problem formulation.

Appendix A.1. Shape of the buckling mode and boundary conditions

The theoretical buckling load of a Winkler beam, expressed by Eq. (6), was derived by assuming the following buckled shape [44]:

$$v(x) = c \sin\left(\frac{m\pi x}{l_r}\right) \tag{A.1}$$

Following the energy method, the critical value of the load can be found by minimizing the deformation energy [44],

$$\Delta T = \Delta U_1 + \Delta U_2 \tag{A.2}$$

where Δ_T is the work done by the external forces, ΔU_1 is the internal strain energy associated with the bending, and ΔU_2 is the internal strain energy associated with the subgrade deformation.

This expression can be rewritten in function of the buckled shape:

$$\frac{N}{2}\int_0^{l_r} v'(x)^2 dx = \frac{EI}{2}\int_0^{l_r} v''(x)^2 dx + \frac{c_h}{2}\int_0^{l_r} v^2(x) dx \tag{A.3}$$

where, in case of the sinusoidal expression of Eq.(A.1) , the integrals can be written as:

$$\int_0^{l_r} v'(x)^2 dx = c^2\frac{m^2\pi^2}{2l_r} \qquad \int_0^{l_r} v''(x)^2 dx = c^2\frac{m^4\pi^4}{2l_r^3} \qquad \int_0^{l_r} v^2(x) dx = c^2\frac{l_r}{2} \tag{A.4}$$

Eq.(A.3) can be solved with respect to the applied load N, yielding the buckling load of a Winkler beam [44]:

$$N_w = \frac{\pi^2 EI}{l_r^2}\left(m^2 + \frac{c_h l_r^4}{m^2\pi^4 EI}\right) \tag{A.5}$$

where m is a positive integer number, indicating the number of half-waves of the sine function along the length of the bar. Note that a sine function with an integer number of half-waves fulfils the pinned-pinned boundary conditions.

The value of m associated with the first critical buckling load is determined by minimizing N_w in Eq. (A.5). This is done by setting the first derivative equal to zero:

$$m^4 - \frac{c_h l_r^4}{\pi^4 EI} = 0 \tag{A.6}$$

from which we obtain the expression

$$m = \frac{l_r}{\pi} \left(\frac{c_h}{EI} \right)^{1/4} \tag{A.7}$$

By substitution into Eq. (A.6), the critical load $N_{ki} = 2\sqrt{c_h EI}$ is derived.

In general, Eq. (A.7) does not give as a solution an integer number. Therefore, the expression of N_{ki} is associated with an inconsistent buckled mode that violates the boundary conditions, being m a real number instead of a positive integer number. Strictly speaking, its value should be determined as the closest integer (lower or greater) that provides the minimum value for N_w. Nevertheless, as reported in [64], the gap between the exact value of N_w and the approximation N_{ki} decreases with increasing values of m. Hence, especially for slender beams such as the screws, the difference between the two predictions can be neglected.

The authors calculated the values of the axial resistance and buckling load as a function of the diameter and threaded length of the screw using Eq. (6) and Eq. (A.5). Fig. A.15 shows the contour plot of the axial resistance using Eq. (6) (a) and Eq. (A.5) (b) for the prediction of the theoretical buckling load. The comparison between Figs. A.15(a) and (b) proves that the difference between N_w and N_{ki} is negligible.

Appendix A.2. Notes on the effect of a variable axial force

Another relevant approximation of Eq. (6) and Eq. (A.5) is the assumption of a constant axial force along the screw. This is not true since only the head of the screw is directly loaded, while the tip cannot be in equilibrium with axial forces (Fig. A.16). Therefore, the axial force decreases along the screw length. This is also evident from the

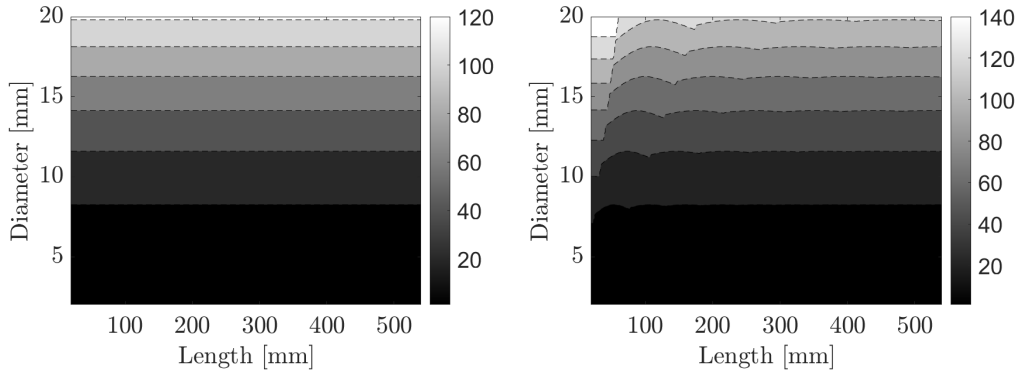

Figure A.15: Countour plot of the axial resistance using Eq. (6) (a) and Eq. (A.5) (b) for the prediction of the theoretical buckling load.

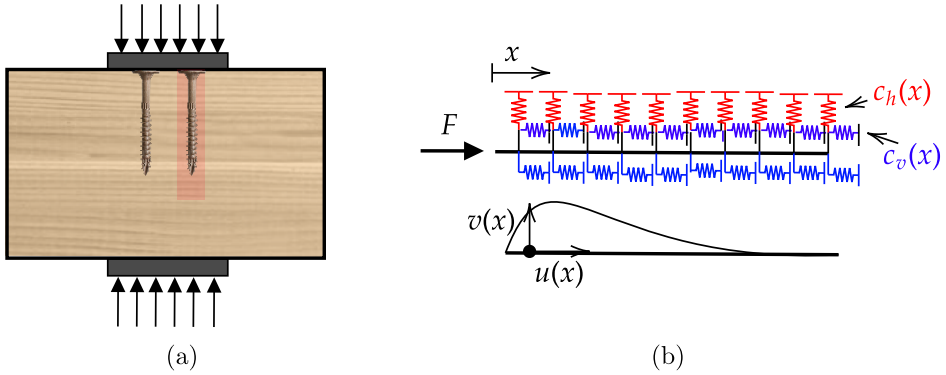

Figure A.16: (a) Illustration of the load application from the steel plate in CPG problems; (b) Mathematical model of the screw under axial forces.

observed failure mode, in which the deformation is concentrated at the screw head, where the axial force is higher.

However, as noted by Bejtka [1], a rigorous mathematical formulation for the buckling of screws is too demanding in complexity and computational effort. Therefore, Bejtka, acknowledging the fallacy of Eq. (A.5), replaced Eq. (6) with the buckling load from finite element analyses in Ansys. The researcher compiled several tables as a function of the diameter and the length, where intermediate values can be estimated with linear interpolation. Despite the merit of this study, tables of values are often difficult to handle, and a closed-form expression for the buckling load should be preferred. Therefore, despite all limitations, the EC5 proposal adopts Eq. (6) rather than tabular values.

In summary, the main limitations of the investigation of Bejtka are the following:

- The author does not consider a screw length higher than 240mm. However, screws can be longer than that. Instability problems often slip common sense and the

suitability of linear interpolations. The complexity of these problems demands the exploration of all the parameter domains to assess the presence of unique regions where the solution could be different than expected from inter and extrapolation.

- Using tabular values is not suitable for standard implementation.

Therefore, the analysis of Bejtka does not allow properly evaluating the error associated with using Eq. (6) due to the reduced number of values reported in the table and the limited extent of the domain.

The actual trend of the axial force can be approximately estimated from the following differential equation describing the axial equilibrium of the screw:

$$u''(x) + \beta^2 u(x) = 0; \;\; \beta = \sqrt{\frac{c_v}{EA}} \tag{A.8}$$

where $u(x)$ is the axial displacement, c_v is the vertical stiffness of the elastic subgrade, and EA is the axial stiffness. The general solution is

$$u(x) = c_1 \sin \beta x + c_2 \cos \beta x \tag{A.9}$$

The boundary value problem can be solved by imposing the following boundary conditions:

$$EAu'(0) = F; \quad EAu'(l_r) = 0 \tag{A.10}$$

The expression for the axial force as a function of x is:

$$N(x) = F\left(\cos \beta x - \cot \beta l_r \sin \beta x\right) \tag{A.11}$$

The accuracy of $N(x)$ and consequently of β mostly depends on c_v, which possesses the primary source of uncertainty. As written in the introduction, there are multiple expressions for the axial capacity of the screw. For instance, Bejtka [1] proposed the following empirical regression for c_v, labelled $c_{v,exp}$.

$$c_{v,exp} = 234 \frac{(\rho d)^{0.2}}{l_r^{0.6}} \tag{A.12}$$

The applicability of Eq. (A.12) in Eq. (A.11) is further examined in Appendix B.

Fig. A.17 shows the contour plot of β for different diameters and screw lengths using Eq. (A.12), Young's modulus for steel equal to 210 GPa and wood density equal to 400 kg/m^3. Parameter β varies between almost 5 and 30 for short screws with a small diameter. In all practical cases, β is lower than 5. These values are associated with an almost linear distribution of N. Conversely, values higher than ten lead to a significant increment of the axial force compared to the one at $x = 0$. It must be remarked that in all design circumstances, the trend of $N(x)$ is almost linear.

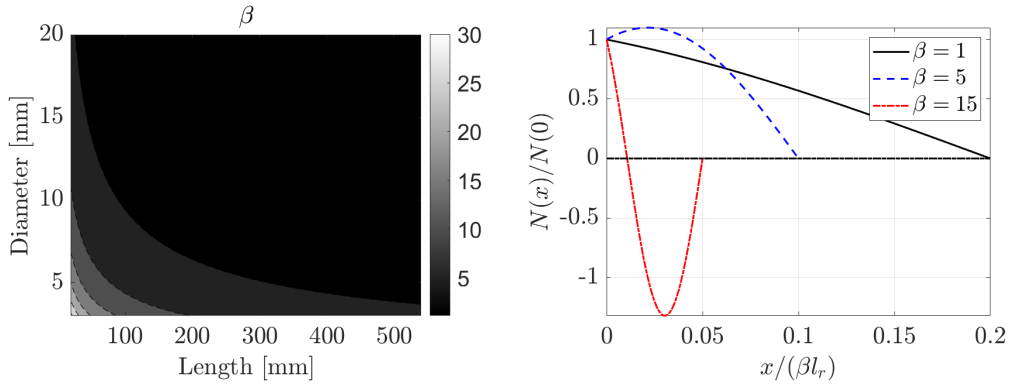

Figure A.17: Contour plot of $\beta = c_v/EA$ and of the variation of the adimensional axial force in Eq. (A.11).

In light of the above, a rigorous buckling model should consider the variation of the axial force along the screw axis. However, this problem can not be treated from an analytical standpoint [69–73]. In fact, there are still no closed-form solutions available in the literature. Hence, in the present work, we propose that the effect of the variation of $N(x)$ is directly considered in the deformed shape of the screw by assuming a damped sine as buckled configuration (see Section 4).

In other words, the main effect of the concentration of axial force at the head of the screw is to produce a buckling mode well approximated by a damped sine. In this way, the axial contribution to the strain energy can still be neglected, and the effect of the variation of axial force is already included in the deformed shape. Hence, in Section 4, the axial force in the energy method is kept constant.

The axial stiffness of the elastic medium (c_v) was obtained by Bejtka [1] by dividing

the axial stiffness of the screw (K_{ax}) by the length of the screw (l_r) as follows:

$$K_{ax} = c_{v,exp} \cdot l_r = \frac{F}{u(l_r)} \tag{A.13}$$

where K_{ax} was derived experimentally by dividing the applied force at the tip (F) and the measured displacement at the head $u(l_r)$, assuming $x = 0$ at the load application point. Eq. (A.11) reveals that the axial force is not constant (see Eq.A.11). Rigorously the stiffness of the screw, obtained by dividing the applied force by the measured displacement at the head, can be written as:

$$K_{ax} = \frac{F}{u(l_r)} = \beta EA \sin(\beta l_r) \tag{A.14}$$

The values of c_v were experimentally derived in [52] with short screws. Thus, the following approximation holds in (A.14), $\sin(\beta l_r) \approx \beta l_r$. Accordingly, the K_{ax} can be approximated by:

$$K_{ax} \approx \beta^2 l_r EA = c_v l_r \tag{A.15}$$

Therefore, by equaling Eq.(A.13) with Eq.(A.15), the following holds $c_v \approx c_{v,exp}$. It must be remarked that this approximation can be considered valid only if $c_{v,exp}$ is derived experimentally with short screws, where $\sin(\beta l_r) \approx \beta l_r$. Then the value of $c_{v,exp}$ obtained for shorter screws can be used in the analysis also when dealing with longer screws.

Appendix A.3. Note on the choice of the boundary conditions

The buckling load reported in the EC5 draft is $N_{ki} = \sqrt{c_h EI}$, which is precisely half of the expression of Eq. (6). As observed by Bejtka [24], this expression approximately corresponds to the theoretical buckling load for elastic beams with free ends embedded in an elastic foundation, which is in good agreement with the FE simulations where these boundary conditions are adopted. This leads to almost half of the buckling load in Eq. (6), as shown in Tab. A.12.

However, in many practical circumstances, when friction forces arise between the screw and the steel plate, the lateral displacement of the head of the screw can be considered negligible (also in agreement with the experimental evidence observed in the Torx test). In this case, assuming a constant vertical load, the theoretical buckling load for double

Table A.12: Comparison between pinned-head and free-head buckling and failure load according to finite element models

Config.	$N_{fem,buck}$ [kN]	$N_{fem,buck}$	ratio	$F_{fem,\mathrm{NLSIM}}$	$F_{fem,\mathrm{NLSIM}}$ [kN]	ratio
Boundary	pinned	free		pinned	free	
T-7.0-160	73.0	30.6	0.42	23.3	19.7	0.85
T-8.2-160	109.7	44.1	0.40	32.3	29.8	0.92
T-8.0-160	99.5	41.1	0.41	30.7	26.9	0.88
T-8.0-180	97.3	40.7	0.42	30.5	25.5	0.84
T-8.0-200	95.6	40.5	0.42	30.3	25.1	0.83
T-8.0-300	90.6	39.7	0.44	29.2	22.9	0.78
T-8.0-340	89.4	39.5	0.44	28.8	22.1	0.77
T-9.0-440	113.7	50.4	0.44	35.9	27.0	0.75

pinned elastic beams embedded in an elastic foundation is $N_{ki} = 2\sqrt{c_h EI}$, which is the one reported in Eq. (6). The buckling shapes associated with these two boundary conditions are compared in Fig. A.18. It is worth reminding, according to [44], that the theoretical

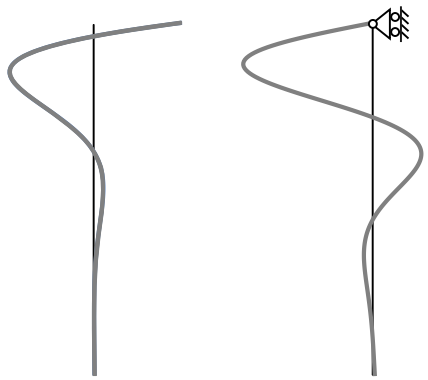

Figure A.18: Buckling shapes of (a) free-head screw and (b) hinged-head screw.

solution of Eq. (6) assumes a sinusoidal buckling shape, while in this paper, the theoretical expression of Eq. (17) is derived with a buckling shape of the form of Fig. A.18(b), coherently with the experimental evidence.